A&A 371, 1137–1149 (2001)
DOI: 10.1051/0004-6361:20010426

Astronomy & Astrophysics

The nature of network oscillations

D. Banerjee[1], E. O'Shea[2], J. G. Doyle[3], and M. Goossens[1]

[1] Centre for Plasma Astrophysics, Katholieke Universiteit Leuven, Celestijnenlaan 200B, 3001 Heverlee, Belgium
[2] ESA Space Science Department, ESTEC Solar System Division, Keplerlaan 1, 2201 AZ, Noordwijk, The Netherlands
[3] Armagh Observatory, College Hill, Armagh BT61 9DG, N. Ireland
e-mail: eoshea@so.estec.esa.nl; jgd@star.arm.ac.uk; marcel.goossens@wis.kuleuven.ac.be

Received 10 January 2001 / Accepted 15 March 2001

Abstract. We examine time-series of spectral data obtained from the Coronal Diagnostic Spectrometer (CDS) and the Solar Ultraviolet Measurements of Emitted Radiation instrument (SUMER) onboard the Solar Heliospheric Observatory (SOHO) spacecraft, in the period 30–31 July 1996. The observations were obtained in lines, ranging in temperature from 12 000 K to 10^6 K, covering the low chromosphere to the corona. We report here on a time series analysis, using wavelet methods, of small individual network regions in the quiet Sun. The wavelet analysis allows us to derive the duration as well as the periods of the oscillations. The statistical significance of the oscillations was estimated by using a randomisation method. The oscillations are considered to be due to waves, which are produced in short bursts with coherence times of about 10–20 min. The low chromospheric and transition region lines show intensity and velocity power in the 2–4 mHz range. The coronal line Mg X does not show any statistically significant power in this range. In general, it is thought likely that the chromosphere and possibly the transition region oscillates in response to forcing by the p-modes, but they are also influenced strongly by the presence of magnetic fields. The observed 2–4 mHz network oscillations can thus be interpreted in terms of kink and sausage waves propagating upwards along thin magnetic flux tubes. We perform a linear numerical computation comparing the results with our observations.

Key words. Sun: chromospheric oscillations – Sun: waves

1. Introduction

It is now established that the solar photosphere is permeated with strong magnetic fields in the form of flux tubes, which occur preferentially in the network, at the boundaries of the supergranular cells on the disk (Stenflo 1994). In the photosphere these magnetic elements are observed in the intergranular lanes as network bright points (Muller et al. 1994; Berger et al. 1995) with typical diameters of 100 km. It is widely accepted now that the physics on these cell boundaries (hereafter we call them the network) differs from that in the interior of the supergranular cells (hereafter, the internetwork). Several authors have reported that the chromosphere in the magnetic network of the quiet Sun oscillates with a frequency close to 3 mHz or even at lower frequencies (Damé et al. 1984; Deubner & Fleck 1990; Kneer & von Uexküll 1993; Lites et al. 1993; Steffens et al. 1997; Curdt & Heinzel 1998; Hansteen et al. 2000), whereas the internetwork seems to oscillate with a dominant frequency of 5.5 mHz (3 min) and oscillations can extend up to 10 mHz and beyond (Hansteen et al. 2000). In order to study the properties of the atmosphere, it is important to concentrate on the dynamics, e.g. the nature of the waves and the origin of the periods observed. Recently Wikstol et al. (2000) and Hansteen et al. (2000) have presented detailed results for the internetwork regions of the quiet Sun. In this paper we will primarily concentrate on the network regions.

A magnetic flux tube supports several kinds of magnetic body waves, namely torsional waves and transverse and longitudinal magneto-acoustic waves (the latter two are also called kink and sausage waves, respectively). The torsional waves (Alfvén waves) are non-dispersive and propagate for any frequency. These waves do not show any Doppler motion at disk centre, although this depends on the line-of-sight direction. The two magneto-acoustic waves are dispersive and can propagate only when their frequencies are above the respective cut-off frequencies. They are evanescent for the frequencies below the cut-off frequency. The propagation of the kink and sausage waves within a thin flux tube in a gravitationally stratified atmosphere and that of plane sound waves in a field-free medium are described by the Klein-Gordon equation (Rae & Roberts 1982; Roberts & Ulmschneider 1997).

Send offprint requests to: D. Banerjee,
e-mail: dipu@wis.kuleuven.ac.be

Table 1. A log of the data sets used in this paper obtained during July 1996

Date	Data set	Instrument	Slit (arcsec)	Pointing X, Y	Start UT	End UT	Lines used
30 July 1996	s3880r00	CDS	4 × 240	+16, −8	14:54	16:19	O III 599 Å, O V 630 Å
30 July 1996	s3883r01	CDS	4 × 118	+61, −9	20:12	20:59	Mg X 625 Å
31 July 1996	203939	SUMER	1 × 300	+54,0	20:39	21:17	O VI 1037.6 Å, C II 1037 Å
31 July 1996	224750	SUMER	1 × 300	+84,0	22:47	23:49	N I 1319 Å, C II 1335 Å

Choudhuri et al. (1993a) pointed out that when the footpoints of the flux tubes move rapidly for a short time, much of the energy is fed into the kink modes at frequencies well above the cut-off frequency and hence can propagate upwards. Kalkofen et al. (1994) have also shown that in the velocity spectrum (see their Fig. 8) there is a high peak at the cut-off with a large amount of energy at higher frequencies.

Until comparatively recently there was no direct observational evidence as to the nature of the foot-point motions. Observations with sub arcsec spatial resolution have revealed that network bright points (believed to be the foot points of thin flux tubes) are in a very dynamic state (Muller et al. 1992, 1994; Berger et al. 1996, 1998; van Ballegooijen et al. 1998). These network bright points exhibit random motions with a broad velocity distribution. Based on high resolution images of the solar photosphere, obtained at the Swedish Vacuum tower telescope, Berger & Title (1996) showed that the bright points move in inter-granular lanes and are primarily driven by the evolution of the local granular convection flow field. It has also been observed (Muller et al. 1994) that these bright points occasionally undergo rapid motions with velocities of the order of 3 km s^{-1}, typically lasting for 3 mins. Their histogram shows a mean speed of around 1.5 km s^{-1}. From an analysis of G-band observations, van Ballegooijen et al. (1998) reported that the temporal variation of the bright point velocity had a correlation time of about 100 s. It was suggested by Choudhuri et al. (1993a) that such jerky motions of foot-points could give rise to kink waves in a flux tube. In a followup paper, Choudhuri et al. (1993b) studied how the energy transport to the higher atmosphere is influenced by the temperature jump in the transition layer.

In this paper we use the formulation of Choudhuri et al. (1993b) to perform a linear numerical computation which we will then compare with the results of our observations. In particular, we use the SUMER observations of Doyle et al. (1999) for two lower chromospheric lines, N I 1318 Å (formed at ∼15 000 K) and C II 1335 Å (formed at ∼32 000 K). For higher temperature lines we have selected some data sets from O'Shea (1997). We have also chosen some of the CDS data sets which have already been discussed in detail by Doyle et al. (1998). Their results indicate that there is power below 4 mHz everywhere along the slit, but that the clearest periods do not always come from the most intense regions. In this paper we only concentrate on the network regions. We have revisited these data sets for two primary reasons. Firstly, while they have used Fourier techniques for power analysis, we now use wavelet analysis. This allows us to study the duration of any statistically significant oscillations as well as their periods. We show that the network oscillations are bursty and intermittent in nature with a finite life time of ∼10–20 min, and thus that the wavelet method is one of the best ways of analyzing such time series. Secondly, earlier observers, Doyle et al. (1998), Curdt & Heinzel (1998), Judge et al. (1997), Hansteen et al. (2000) have binned several pixels to achieve a better signal-to-noise ratio and have reported on coherent oscillations. However if one sums adjacent pixels with different phase properties one gets phase mixing. Here we report on the wavelet power analysis of individual pixels (wherever possible) in the network regions of the quiet Sun and compare the results with a linear numerical simulation.

2. Observations and data reduction

The data discussed here were selected from the observing period 30–31 July 1996. The observations are summarised in Table 1. We have used the Coronal Diagnostic Spectrometer (CDS) (Harrison et al. 1995) and Solar Ultraviolet Measurements of Emitted Radiation (SUMER) (Wilhelm et al. 1995) instruments onboard the Solar Heliospheric Observatory (SOHO).

For the CDS data we debiased and flat fielded the data using the standard CDS software procedure VDS_CALIB (see Doyle et al. 1998 for details). The resulting data after running this procedure were in units of photon-events/pixel/sec and multiplying by the exposure time yielded units of photon-events/pixel. These have been termed as "counts" in the results section. The procedure CDS_CLEAN was used to clean the data of cosmic ray hits. Slant and tilt corrections were applied to the data using another CDS software procedure, NIS_ROTATE.

Before beginning our analysis of the SUMER data, we first had to apply the standard SUMER data reduction procedures of flat-fielding and de-stretching. It was not found necessary to apply dead-time and local gain corrections, due to the low count levels involved. All of the data reduction steps involved the use of programs obtained from the SUMER software tree. The different steps involved in the calibration of SUMER data are summarised in the SUMER data reduction cookbook (see SUMER

web-page) and in Pérez (1999). We refer the reader to these publications for further details.

The localised (in time) nature of the wavelet transform allows us to study the duration of any statistically significant oscillations as well as their period. So, to find the most reliable periods, we performed wavelet analysis on the data. By decomposing a time series into time-frequency space, one is able to determine both the dominant modes of variability and how those modes vary in time. We should also point out that wavelet transforms suffer from edge effects at both ends of the time series. The region in which these effects are important are defined by the "cone of influence" (COI) (see Torrence & Compo 1998), and are shown in our plots of the wavelet spectrum as the cross-hatched regions.

The statistical significance of the observed oscillations was estimated by using a Monte Carlo or randomisation method. The advantage of using a randomisation test is that it is distribution-free or non-parametric, i.e. it is not limited or constrained by any specific noise models, such as Poisson, Gaussian etc. We followed the method of Fisher randomisation as outlined in Nemec & Nemec (1985) and implemented in the UK Starlink software package, PERIOD (Dhillon & Privett 1997).

We shall briefly discuss the method used in more detail below. The randomisation test is based on the assumption that, if there is no periodic signal in the time series data, then the measured values (intensity, velocity etc.) are independent of their observation times. For example, the intensities I_1, I_2,... I_n, observed at times t_1,t_2,... t_n, are just as likely to have occurred in any other order $I_{r(1)}$, $I_{r(2)}$,... $I_{r(n)}$, where n is the total number of observations and $r(1)$, $r(2)$,... $r(n)$ is a random permutation of the subscripts 1,2,... n. By using the maximum power peak, at each time location, in the wavelet spectrum as the "test statistic" (see Dhillon & Privett 1997) it was possible to test the hypothesis that there was no periodicity in our data. Ideally this would have been done by evaluating the peak power from the original ordering of the time series data and then comparing it to the peak powers evaluated from the $n!$ equally likely permutations of the time series data. The proportion of permutations that gave a value greater or equal to the peak power of the original time series would then provide an estimate of p, the probability that *no* periodic component is present in the data, i.e. a large value of p suggests that there is little or no real periodicity in the data whereas a small value of p suggests that the measured periodicity is likely to be real. In practise $n!$ is usually so large that it is not possible to do this, due to computational and time constraints, and so the peak powers are generally calculated for only a random sample of m permutations. By carrying out this approximation, for a random sample of 150 permutations, we were able to obtain a reliable *estimate* of p. For a sample of 150 random permutations the standard errors of the p value are no greater than 0.04 (Nemec & Nemec 1985). Of course, the larger the number of permutations chosen, m, the lower the standard error of the p value. The probability levels displayed in this paper are the values of $(1-p)\times 100$, i.e. the percentage probability that periodic components *are* present in the data. We chose a value of 95% as the lowest acceptable probability level. Occasionally the *estimated* p value can have a value of zero, i.e. there being an almost zero chance that the observed time series oscillations could have occurred by chance. In this case, and following Nemec & Nemec (1985), the 95% confidence interval can be obtained by use of the binomial distribution. The confidence interval is given by $0.0 < p < 0.01$, that is, the probability $((1-p)\times 100)$ in this case is between 99–100%.

We should remind the reader that the rotational compensation was not used for any of the temporal series. The data were thus obtained in a sit and stare mode. With the relatively large slit width (4 arcsec) of CDS, the results are not going to be affected over 1 mHz, but in the case of SUMER, the power could be affected up to 2.6 mHz, depending on the size of the source and its location (see Doyle et al. 1998, 1999).

We should also point out that the velocity values presented in this paper are relative velocities, that is they are calculated relative to an averaged profile that was obtained by summing over all pixels along the slit and all time frames. An absolute velocity calibration isn't available, thus the derived velocities reflects only line shifts.

3. Results

3.1. CDS

We present here the results from the CDS data set, s3880r00. We will now show and discuss the behaviour of pixels along the slit, which covers both network and internetwork regions of the Sun. To do this, we show in Figs. 1 and 3, time slices of the observed O III 599 Å and O V 630 Å lines, which are formed at temperatures of 100 000 K and 250 000 K respectively. In these plots, the solar north-south (SOLAR_Y) direction is in the vertical axis, the horizontal axis is time. Note that 143 spatial pixels corresponds to 240 arcsec. To bring out the details of the original intensity map we have filtered out the bright components in the image. The intensity map $I(y,t)$ is convolved in the time direction with a Gaussian $G(t)$. This results in a smoothed image $S(y,t) = I{*}G$ which contains no high frequencies. Then dividing the original intensity map by the smoothed map results in the contrast enhanced map, i.e. $C(y,t) = I(y,t)/S(y,t)$ (see Doyle et al. 1999 for details). The contrast-enhanced images are shown in the left panels of Figs. 1b and 3b. The grey scale coding has the most intense regions as white. The contrast enhanced images show the fluctuations in the bright features more clearly and their appearance seems periodic. These maps also show some grain structures within the network. The total number of counts in a pixel (summed counts) during the observation is shown in the right columns. This is useful in identifying the network boundaries.

Figures 2 and 4 presents spatially resolved intensity and velocity power spectra as a function of position along

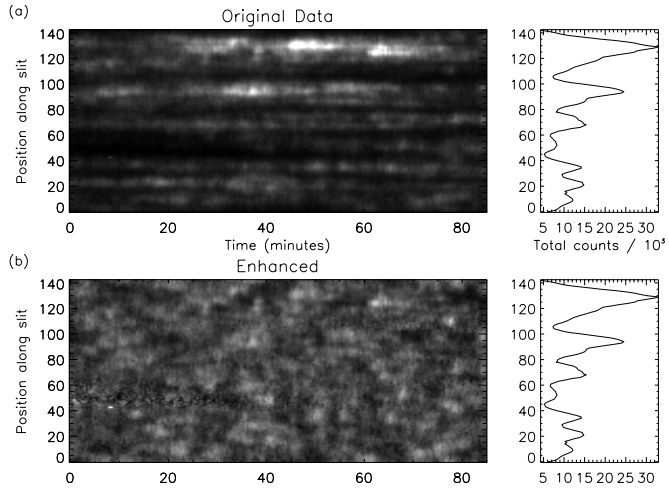

Fig. 1. The space-time behaviour of the intensity in the O III 599 Åline in the s3880r00 data set. The grey scale coding has the most intense regions as white. Panel **a)** represents the original data and **b)** represents the contrast enhanced image. The right panels show the counts summed over all time against the slit locations, which clearly shows the network enhancements

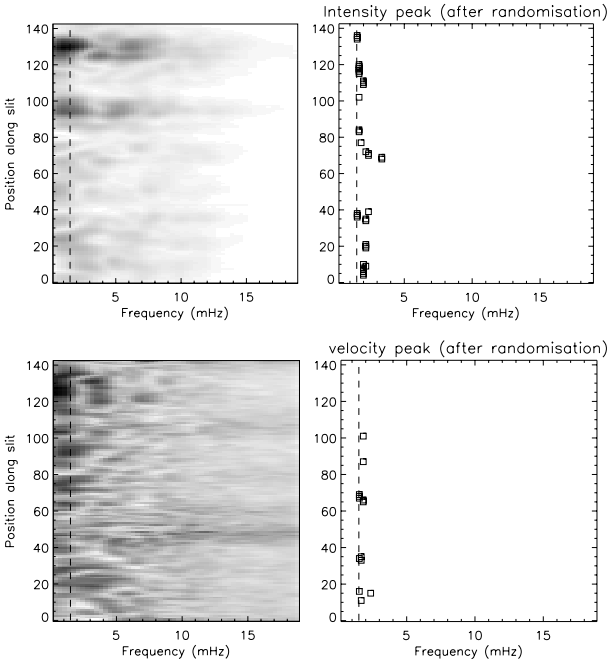

Fig. 2. Power in the intensity (top row) and velocity (bottom row) fluctuations of the O III 599 Å line in the s3880r00 data set, as a function of frequency of oscillation and spatial position along the slit. Left panels show all power for individual pixels, whereas the right panels show the frequencies that correspond to the maximum power above the 95% confidence level, after the randomisation test. The dashed line in all plots shows the value of the cut-off frequency, 1.5 mHz (because of no rotational compensation)

the slit (x-f slice). The grey-scale x-f slices (left panels) show all power before the randomisation test, whereas the frequencies in the right panels (squared boxes) correspond to the maximum power, which have more than the 95%

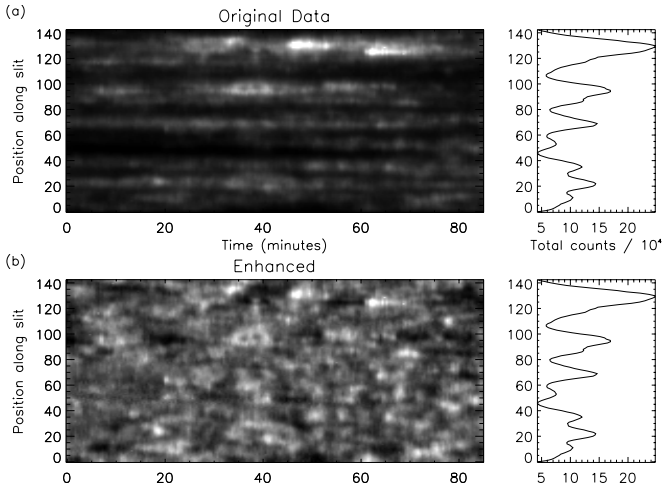

Fig. 3. Same as Fig. 1, but for O V 630 Å line from the same data set, s3880r00

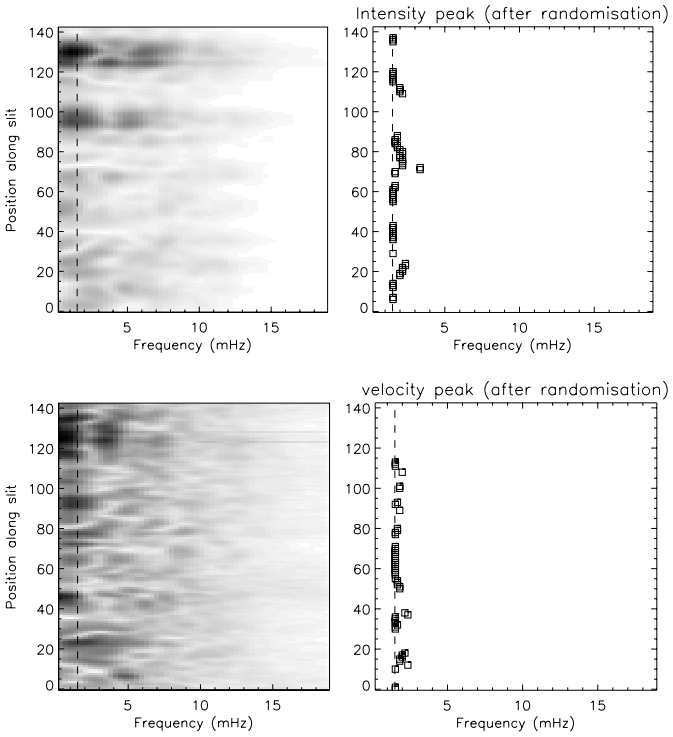

Fig. 4. Same as Fig. 2, but for O V 630 Å line from the same data set, s3880r00

probability level after the randomisation test. The grey-scale plots in Figs. 2 and 4 give an overall impression that there are more velocity oscillations than intensity oscillations. One should pay particular attention to the right panels of Figs. 2 and 4 which show clearly that after the randomisation test for almost all locations, the maximum power is in the 1.5–3 mHz range. Thus one should be very careful in interpreting results such as these while looking at normal power spectra, without a proper noise detection test. We should also remind the reader that since the rotation compensation was turned off, we cannot say anything about frequencies below ∼1.5 mHz.

From Figs. 2 and 4 it appears that the network and internetwork shares frequencies in the 1.5–3 mHz range. We should point out that this is probably due to the low counts present in the internetwork regions. From the x-f slices we have noticed that whenever we have low counts corresponding to a single pixel the randomisation test does not find any power maxima with a high probability level (more than 95%). For an investigation of internetwork behaviour and to compare with recent studies (Cauzzi et al. 2000; Hansteen et al. 2000; Wikstol et al. 2000), we show two representative examples of internetwork behaviour in Figs. 5 and 6. We notice that for the internetwork the velocity oscillation is the dominant oscillation. However for CDS we do not have good velocity resolution and, furthermore, for low signal to noise (particularly for internetwork locations) the velocity does not show reliable oscillations. For this reason we chose one of the SUMER data sets (details will be described in the following section) to show the representative internetwork behaviour. Here we sum over three pixels to improve the signal to noise. For a representative internetwork location (pixels 209-211) we present the wavelet results in Figs. 5 and 6, for N I and C II respectively. In the wavelet spectrum plots the darker contour regions show the locations of the highest power. Therefore the dark contour regions in the wavelet spectrum plots indicate the locations of the most likely frequencies in the time series. The lowest panel shows the variation of the probability level over the observing time, by which it is possible to see whether the power at any time in the wavelet spectrum has a high or low probability of being due to noise. Only locations that have a probability of greater than 95% are regarded as being real, i.e. not due to noise. Cross-hatched regions, on either side of the wavelet spectrum, indicate the "cone of influence", where edge effects become important (see Torrence & Compo 1998). These results show that the intensity oscillations are not strong and that the velocity oscillations are the dominant ones. The frequencies from the velocity oscillations extend well up to ∼10 mHz. In the right panel the global wavelet spectrum, which is just the average of the wavelet power spectrum over time, is plotted. For N I the velocity global spectrum shows a peak around 3.7 mHz, with a secondary peak around 7 mHz, whereas for C II it shows wide distribution of power around 4.5 mHz, with power extending up to 10 mHz.

Recently Cauzzi et al. (2000), Hansteen et al. (2000), Wikstol et al. (2000) have presented a comparative study of the network versus internetwork regions of the quiet Sun. Thus we do not say anything further in this regard, but we will instead now concentrate on individual network pixels and study their detailed properties. We do this because later (in Sect. 4) we will present a numerical model, with which we will then compare the results (frequencies etc.) found in these representative individual network pixels (Sect. 5).

First, we concentrate on pixel 70 of the s3880r00 data set (see Fig. 1 for the location), which corresponds to a network boundary. The results from the wavelet analysis for pixel 70 for the O III 599 Å and O V 630 Å lines, are presented in Figs. 7 and 8 respectively. For the O III line the time frequency phase plane plot of intensity (see Fig. 7a middle panel) shows significant power between 2–4 mHz, with strong peaks around 2.4 mHz and 3.5 mHz. The global wavelet spectrum indicates that on average the dominant power is at 2.4 mHz. The randomisation method was also used to determine the probability of whether the oscillations at this frequency, in the global wavelet spectrum, may be due to noise. From this test we find that this 2.4 mHz oscillation is present at a probability of 99–100%. This information is printed over the global wavelet plot, together with the main frequency present in Fig. 7a. We have used a lower cut off frequency of 1.5 mHz for all the CDS data sets, as below this limit the edge effects and the sit and stare effect could be important. Note that in the wavelet spectrum of the intensity, the power is strong in the time interval 20–40 min and again between the times of 60–80 min. This is also clear from the lowest panel which shows that the probability that the oscillations are real is above the 95% level only within these time intervals. Note that this probability always refers to the max. power in the time frequency phase plot. The velocity does not show significant power within 2–4 mHz for the same pixel position (see Fig. 7b). However, it does show weak power around 1.5 mHz over short periods at the beginning and towards the end of the time series.

The intensity corresponding to O V 630 Å line behaves in the same way as the O III 599 Å line. It shows strong power in the range 1.5–4 mHz (see Fig. 8a), with the strongest peaks at 1.7 mHz and 3.5 mHz. It also shows the bursty nature of the oscillations, whereas the velocity shows a strong peak around 1.5 mHz for the first 20 and again between the 40–80 min of the observing sequence. There is a second peak around 3.5 mHz in the global spectrum. Note that the O V line is much stronger than the O III line, so the fact that the velocity corresponding to O III does not show significant power, may be because of low count rates. It is interesting to note that the brightest network regions (corresponding to the region around pixel 130) do not show significant oscillations above 1.5 mHz. From Figs. 1 and 3 we can further speculate that in this location probably we have detected a much more dynamic phenomenon like a *blinker*, whose appearance has masked the background oscillation.

Next we will focus on the s3883r01 data set. Here 70 spatial pixels correspond to 118 arcsec. We present results of a network region as seen from the Mg X 625 Å line (formed at 10^6 K) in Fig. 9. Because of low count rates, in this case, we are forced to sum over four pixels, namely pixels 39–42. The lower panels indicating the probability levels allow us to conclude that we do not have any significant oscillations corresponding to this line even though the standard wavelet spectrum may give a false impression that there is power at ∼6 mHz and above 10 mHz. Thus for low count statistics it is very important to have a probability level test before concluding the presence of power, particularly if the signal-to-noise ratio is low.

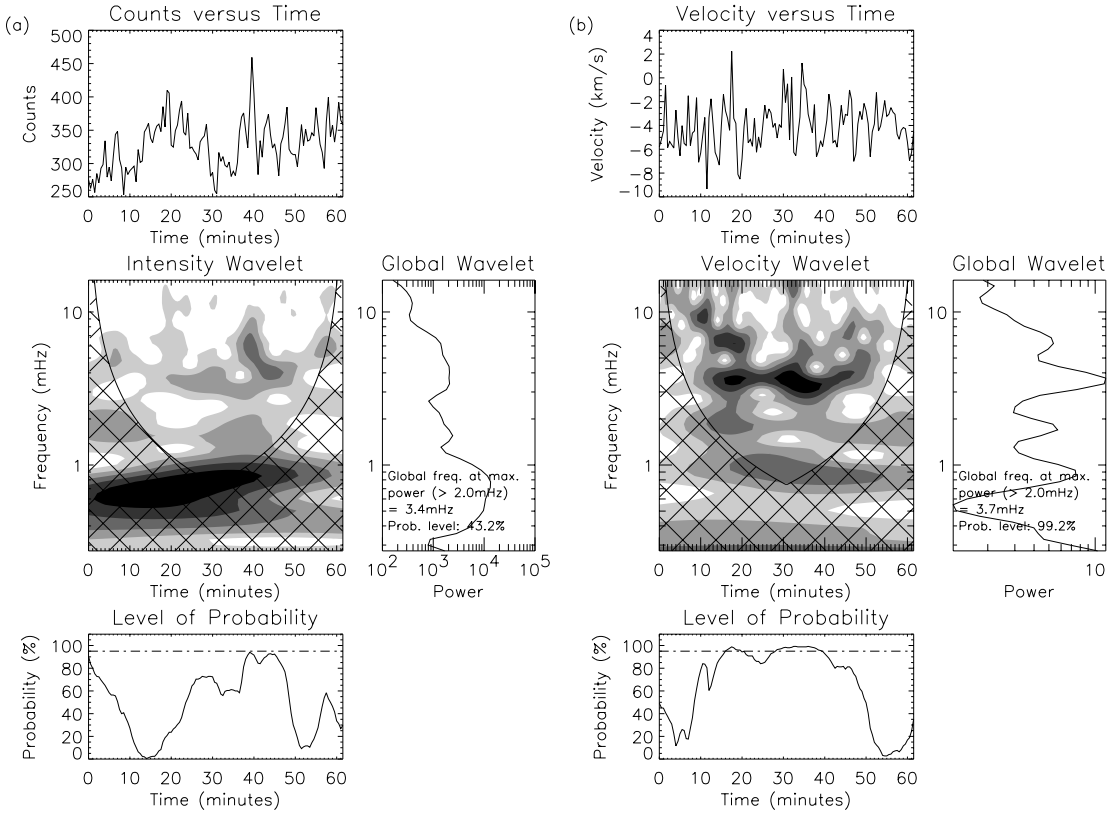

Fig. 5. Wavelet results, corresponding to a internetwork location (pxs 209-211) of the 31st July data set for the N I 1319 Å line (see Fig. 1 of Doyle et al. 1999 for location). Panels **a)**, **b)** represent intensity and velocity results respectively. The middle left panels show the time frequency phase plot corresponding to the variations shown in the top panels. The middle right hand panels show the average of the wavelet power spectrum over time, i.e. the global wavelet spectrum. The lowest panels show the variation of the probability from the randomisation test

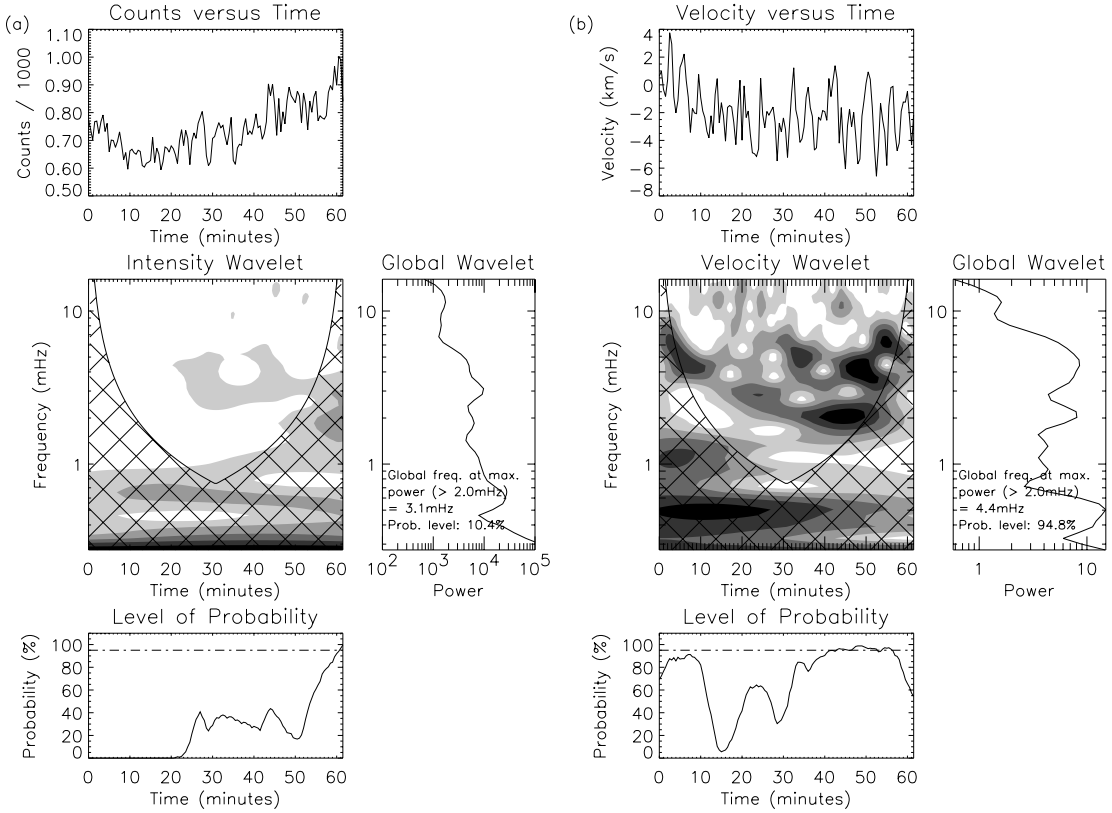

Fig. 6. Same as Fig. 5, but for C II 1335 Å line corresponding to an internetwork location and data set as Fig. 5

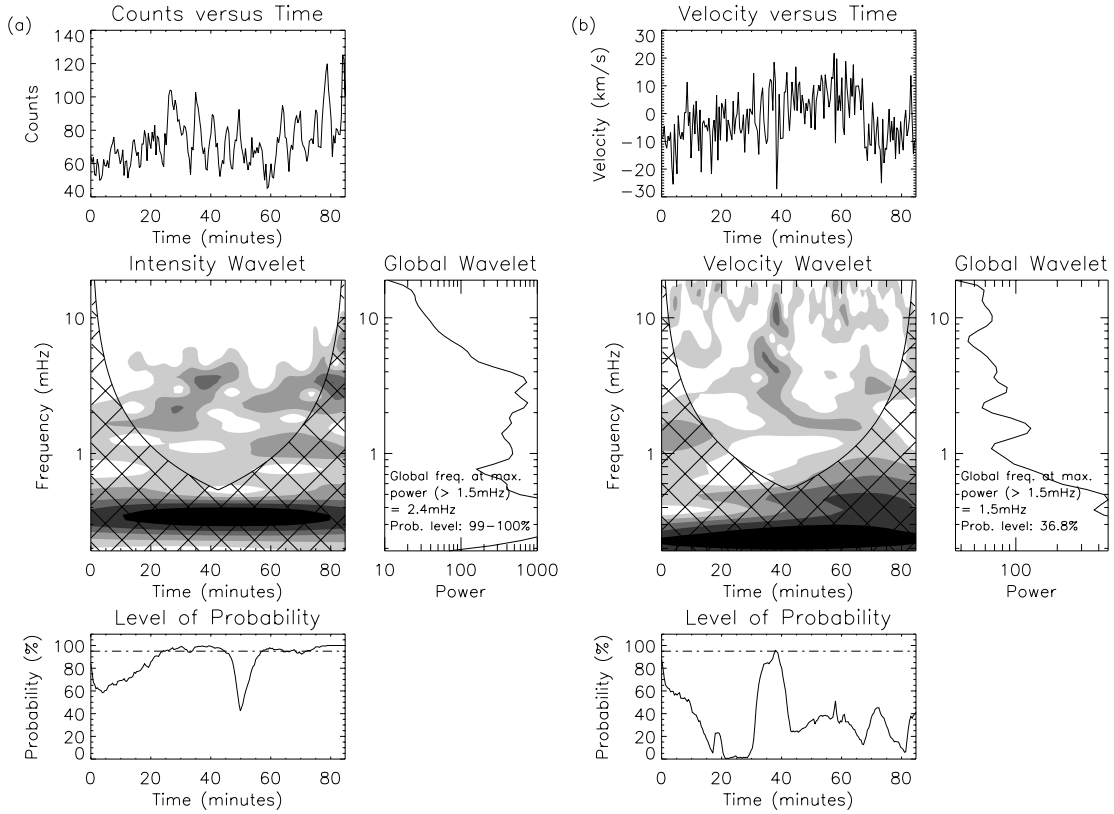

Fig. 7. A typical network region, corresponding to pixel 70 of the s3880r00 data set for the O III 599 Å line (see Fig. 1 for location). The results of the wavelet analysis for the intensity and velocity are shown in panels **a)** and **b)** respectively

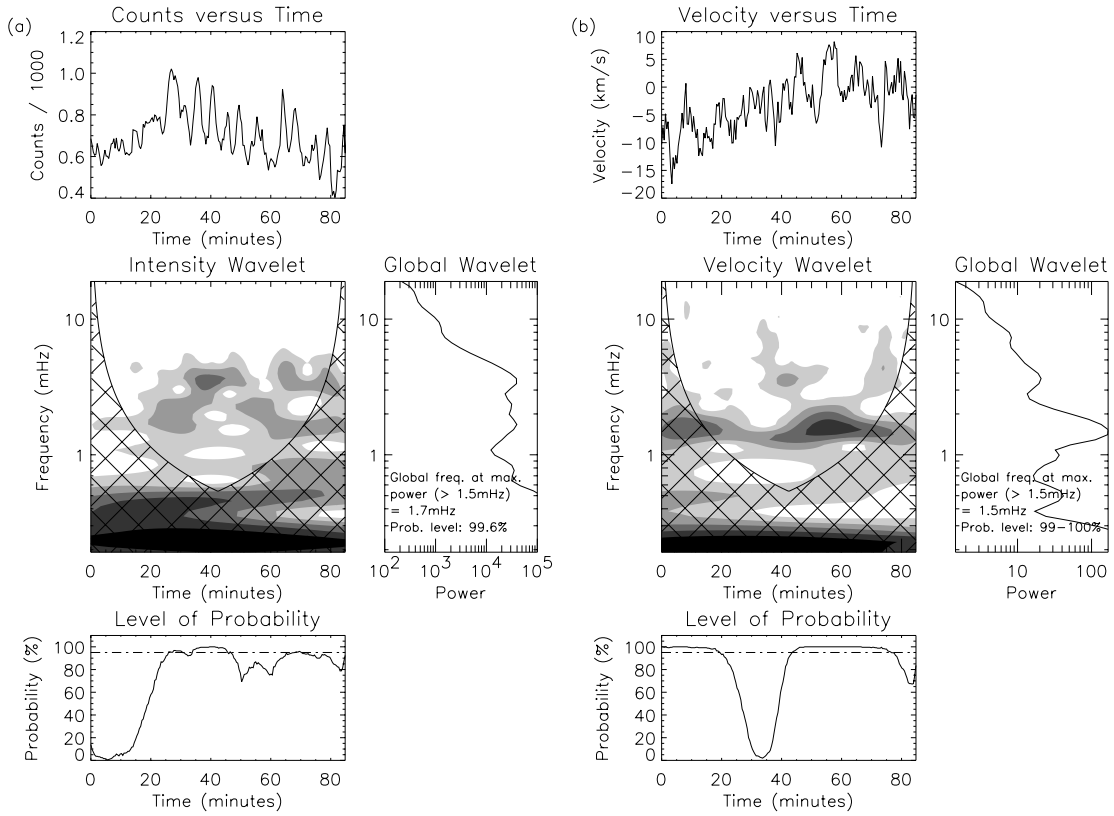

Fig. 8. Corresponds to pixel 70 of the s3880r00 data set and O V 630 Å line. Representations are the same as Fig. 7

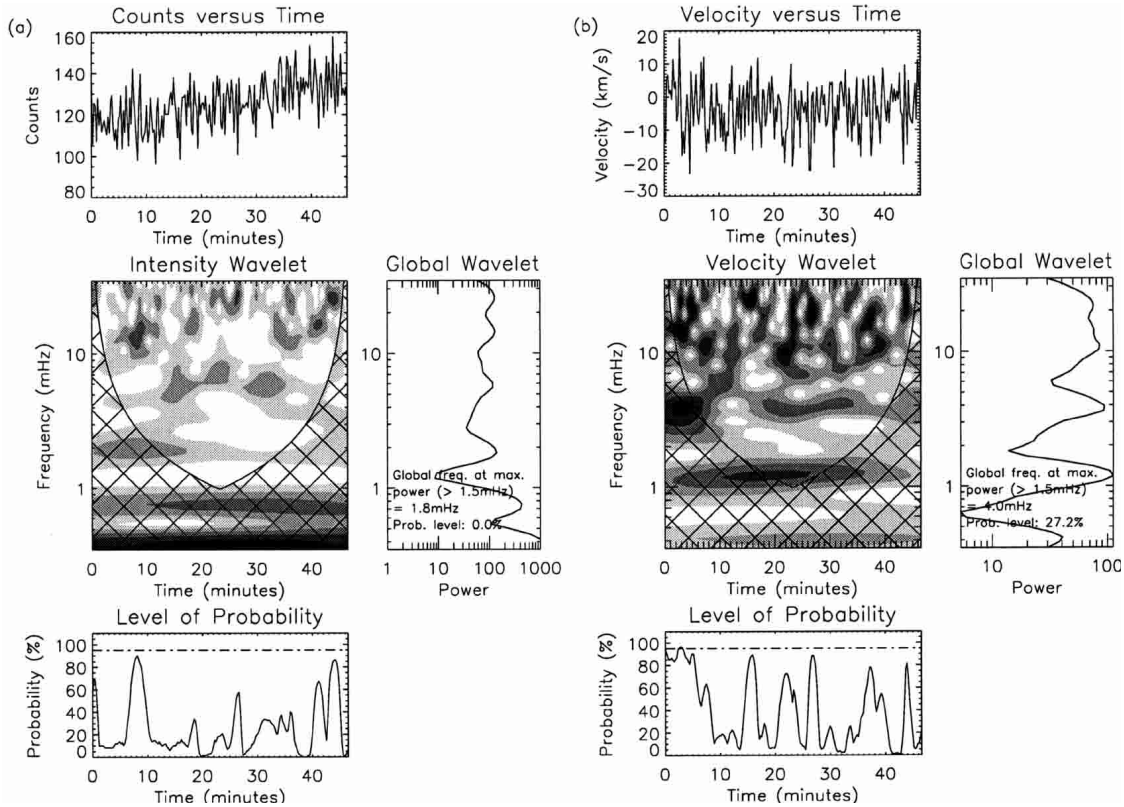

Fig. 9. Wavelet results corresponding to the Mg X 625 Å line of s3883r01. To improve the signal to noise, we binned by four pixels (namely pixels 39–42) along the slit, in effect creating new pixels of 5×4 arcsec^2

The oxygen lines in this data set, as in the others, show power within the 2–4 mHz range, intermittently for the network pixels, but do not show any power above 5 mHz.

3.2. SUMER

The details of these observations with detailed analysis of all the regions can be found in O'Shea (1997) and Doyle et al. (1999). In this paper we select some network pixels and concentrate on the wavelet analysis only. We recall that SUMER has a better spatial resolution than CDS, here 1 pixel ∼1 arcsec, whereas in CDS, 1 pixel ∼1.68 arcsec. For all SUMER data sets we have used a cut-off frequency of 2.0 mHz, as below this limit the edge effect and sit and stare effects can be important.

First, we present results of a data set taken on 31 July (see Table 1) for the two lower chromospheric lines (N I 1319 Å and C II 1335 Å). We concentrate on network pixel 168 and present the wavelet results in Figs. 10 and 11 for N I and C II respectively. For N I the intensity and velocity shows maximum power around 3.7 mHz, with a weaker peak around 2 mHz, although with a low probability (∼75%) for the intensity oscillations. It also shows the intermittent nature of the network oscillations, with typical life times of 10–15 min. Considerable blue shifts are also noted for N I (see top panel of Fig. 10b). For C II we find considerable power in the intensity, with a strong peak at 2.6 mHz, using the global wavelet spectrum. The velocity on the other hand shows strong power around 2.0 mHz for the 30–50th minute of the observing period.

Finally we present results for the data set taken on 31 July '96 with the C II 1037 Å and O VI 1037.6 Å lines (see Table 1). We present the wavelet results corresponding to network pixel 166, in Figs. 12 and 13 for C II and O VI respectively. Both the intensity and the velocity of the C II line show very strong power around 2.5 mHz, with a lifetime of the order of 20 min. The O VI line also shows similar behaviour. The intensity and velocity shows strong power at 2.0 and 2.4 mHz respectively over almost the entire observing period with a very high percentage probability level. We should point out here that with the overlay of the magnetogram with the SUMER slit position, we found definite presence of magnetic field at this network pixel. Note that Cauzzi et al. (2000) have shown that all the network bright points in their NaD_2 images are co-spatial, within 1 arcsec, with locations of enhanced magnetic field. In our particular case we strongly feel that the oscillations are influenced by the presence of magnetic fields.

4. Numerical model

A number of authors have proposed that the corona is heated by transverse tube or kink waves (Spruit 1981;

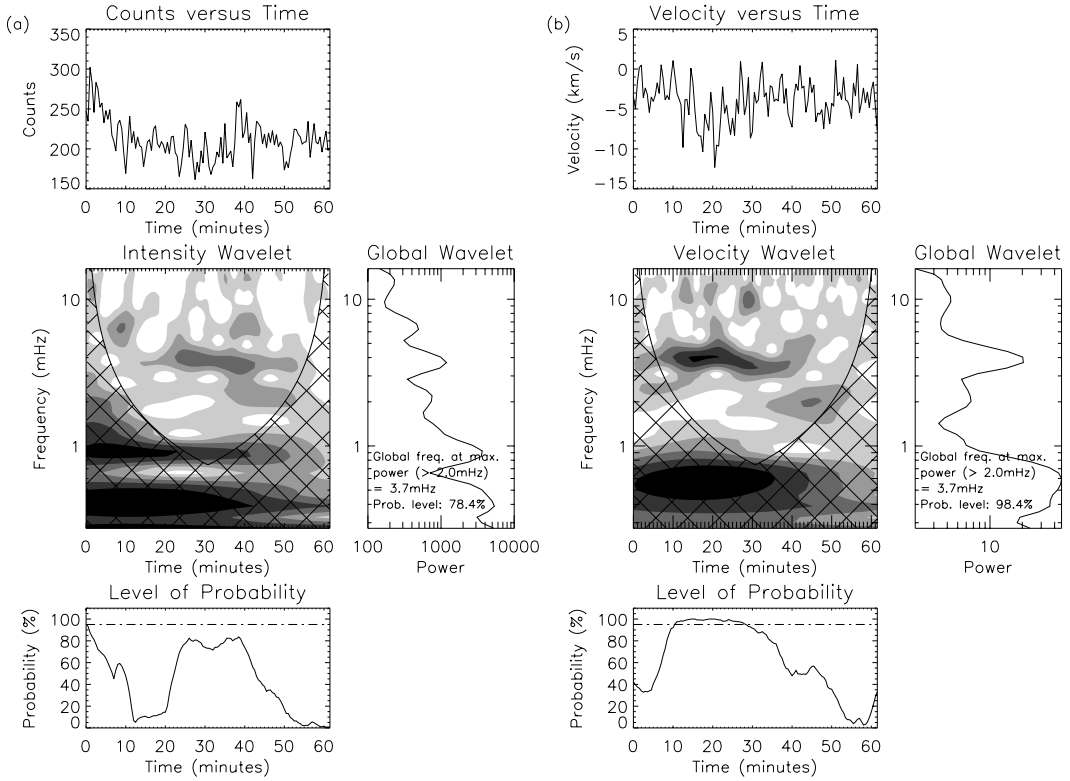

Fig. 10. Wavelet results, corresponding to a network pixel 168 of the 31st July data set for the N I 1319 Å line (see Fig. 1 of Doyle et al. 1999 for location). Panels **a)**, **b)** represent intensity and velocity results respectively

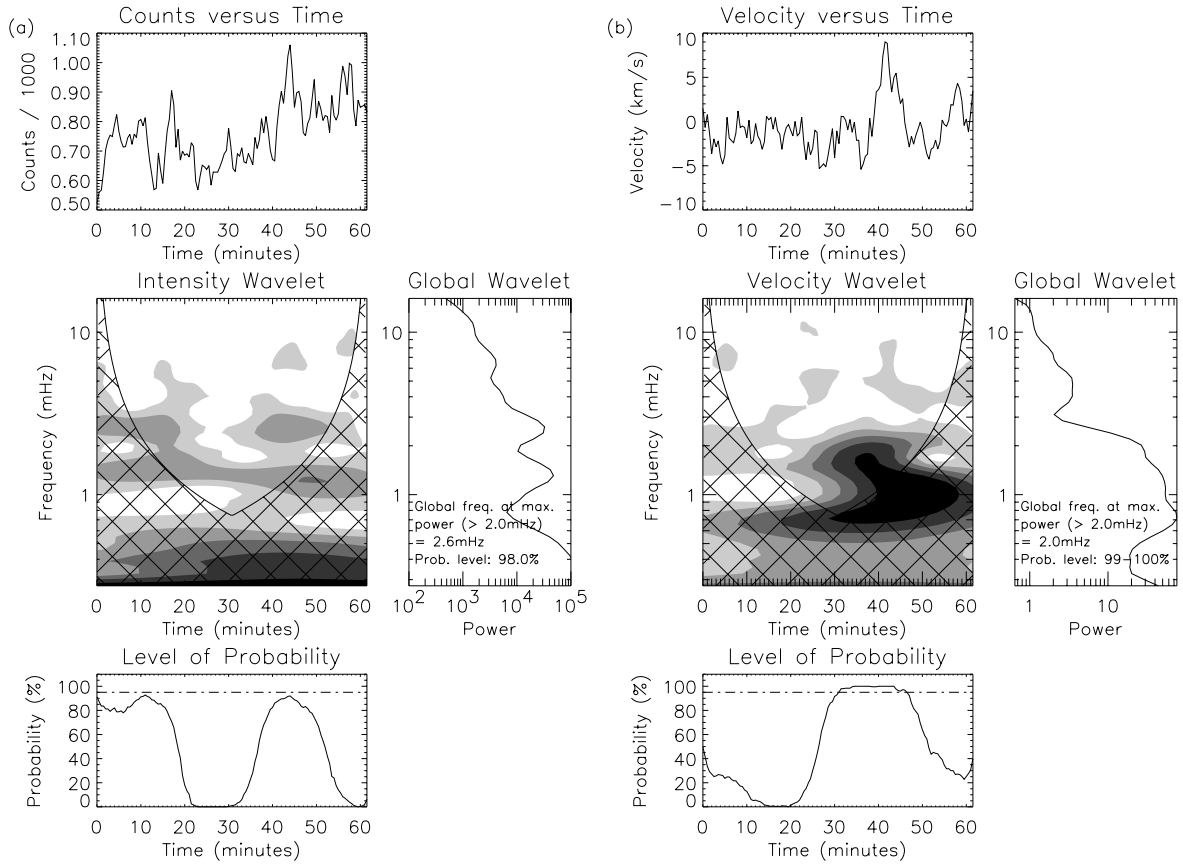

Fig. 11. Same as Fig. 10, but for C II 1335 Å line corresponding to the same pixel position and data set as Fig. 10

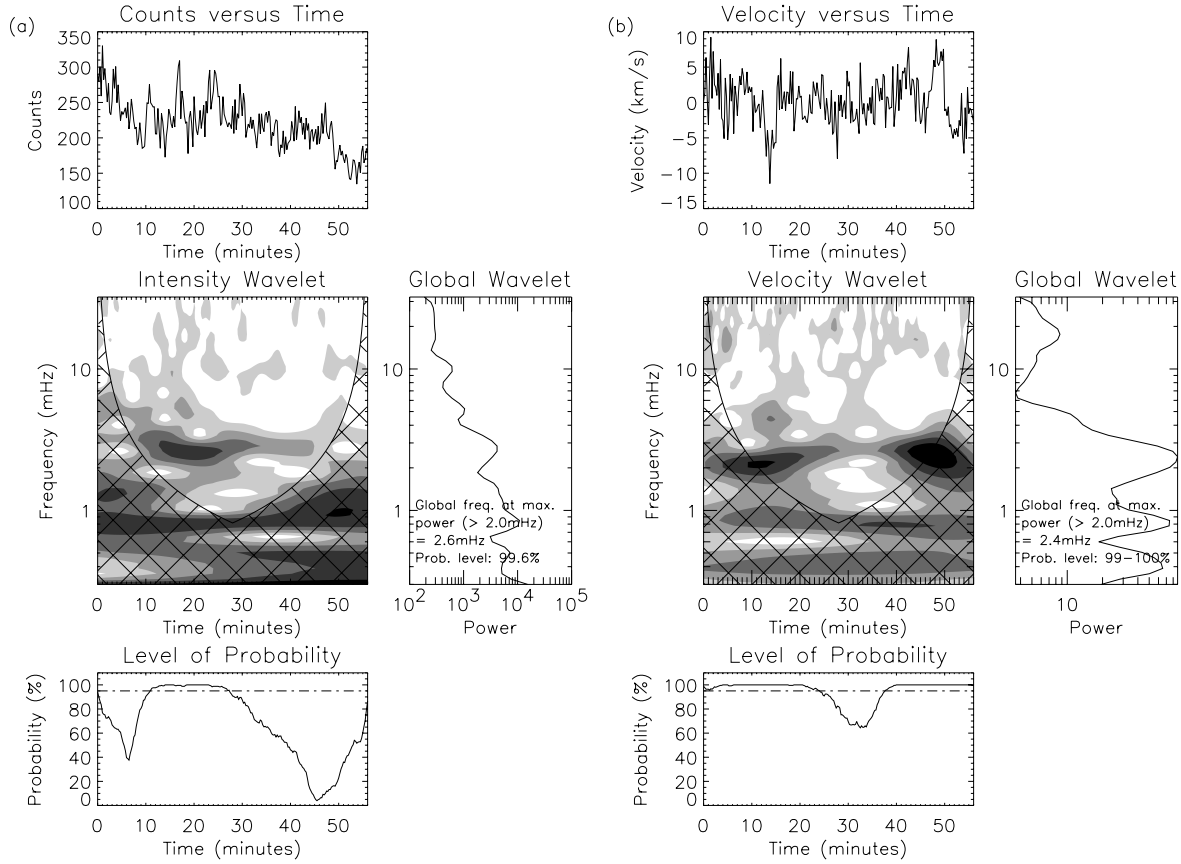

Fig. 12. Wavelet results corresponding to pixel 166 of the 31st July data set for the C II 1037 Å line

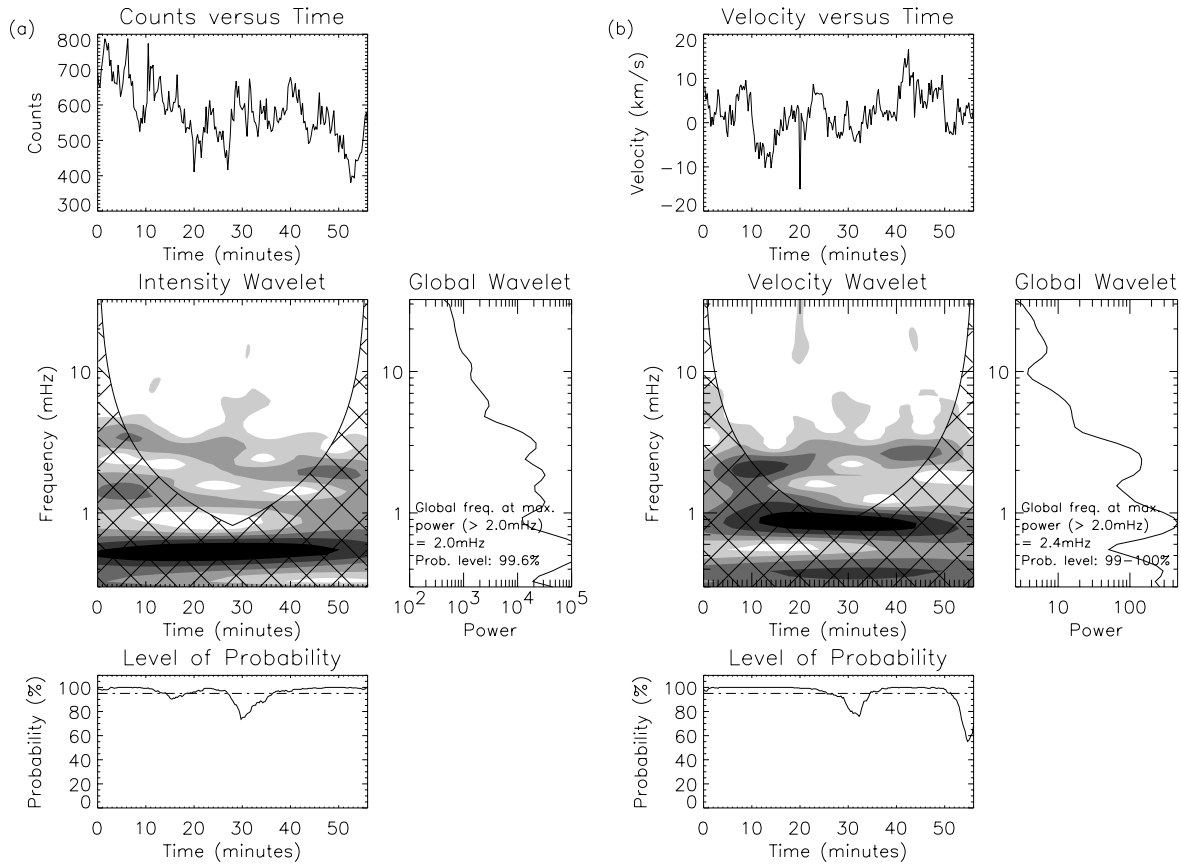

Fig. 13. Same as Fig. 12, but for O VI 1037 Å line corresponding to the same pixel position and data set as Fig. 12

Choudhuri et al. 1993a,b). Muller et al. (1994) have reported a mean speed of the network bright points of 1.4 km s^{-1} and concluded that there is significant energy in these motions to heat the quiet corona. Hasan & Kalkofen (1999) have argued that network oscillations can be efficiently excited through the buffeting action of external granules on flux tubes with intermittent motions (of about 2 km s^{-1}) occurring on a time scale of less than about half the cut-off period of the kink waves.

In this section we follow the formalism developed in Choudhuri et al. (1993b) and study the response of the footpoint motions on the propagation of kink waves in an idealized solar atmosphere. We assume that the flux tubes situated in the network boundaries are isothermal and "thin" as compared to the pressure scale-height H. Assuming that the pulse generated by the foot-point motion has a Gaussian velocity profile, and that the kink waves propagate within a thin flux tube embedded in a two-layer isothermal atmosphere, the displacements of the flux tubes at different heights, for a particular maximum velocity of the foot-point motion, is given in Choudhuri et al. (1993b) (see Eqs. 30a,b).

The parameter space is characterized by dimensionless variables, $\tau = \omega_{c_1} t$ (time) and $s = z/4H_1$ (height), where ω_{c_1} is the cut off frequency of the kink waves and H_1 is the scale height of the first layer. The parameter, $\alpha = h/4H_1$ is the measure of the thickness of the first layer, where h is the height of the layer in kilometers, $r = \sqrt{T_1/T_2}$ is the measure of the temperature contrast between the two layers, $\lambda = \frac{v_0}{\omega_{c_1} L}$ is a measure of the strength of the footpoint motion, where L is a typical displacement of the flux tube, and v_0 is the maximum velocity of the foot-point (see Choudhuri et al. 1993b for details). Fontela et al. (1990) showed that a two-layer model is a good representation of the solar atmosphere. For an idealized solar atmosphere and choosing the parameter space to compare with our observations we have $\beta = 0.3$ and $H_1 = 150$ km s^{-1}, which gives $\omega_{c_1} = 0.012$ rad s^{-1} (period = 524 s). The time scale for the footpoint motion is given by $T = L/v_0$. We consider the effect of an average footpoint motion with velocity $v_0 \sim 1.5$ km s^{-1}, a lifetime of the order of 300 s and a typical displacement 450 km. This gives $\lambda = 0.28$. We place the temperature jump around 2000 km ($\alpha = 3.34$) above the photosphere and choose a temperature contrast corresponding to $r = 0.24$ ($T_1 = 6000$ K and $T_2 = 105\,000$ K). Whenever a pulse propagates through a stratified medium, it is known to leave a wake behind it oscillating with the cut-off frequency of the atmosphere (Lamb 1932; Rae & Roberts 1982). Figure 14 shows the oscillations at different heights corresponding to our idealized solar atmospheric model. Note that the periods are only slightly different at different heights of the atmosphere and that the amplitude of oscillation grows as we go higher in the atmosphere. For $z = 1800$ km, which corresponds to a height around the higher chromosphere, the wave amplitude becomes so large that they become non-linear. Thus at these locations the non-linear mode transformation can take place (Ulmschneider et al. 1991). Kalkofen (1997) has mentioned that in the mid-chromosphere the displacement of the flux tube becomes comparable to the diameter of the tube and thus non-linearity has to be taken into account. We will take up this issue in detail in the discussion section. We should point out that the amplitude and life time of these oscillations crucially depend on the magnitude of the velocity of the foot-points. Figure 15 shows the displacement of a flux tube at $z = 1800$ km, corresponding to different values of v_0. For slow Brownian motions ($v \sim 1$ km s^{-1}) the flux tube barely oscillates, but for faster foot-point motions ($v > 3$ km s^{-1}) the amplitude of oscillations is larger but damps more quickly. Furthermore the waves become non-linear at much lower heights. Note that the wake oscillates with a frequency which is neither the cut-off frequency of the lower layer ($\nu_1 = 1.9$ mHz) nor the upper layer ($\nu_2 = 0.46$ mHz). Instead it oscillates with a period =∼390 s ($\nu = 2.56$ mHz). For a single layer solar atmosphere Choudhuri et al. (1993a) have shown the evidence of a wake with the kink characteristic frequency. In a two layer model, however the situation is somewhat more complicated, since each layer has its own characteristic frequency. For different combinations of α and λ, we have found that if the α and λ values are both small, then the wake mainly oscillates with the cut-off frequency of the upper layer (also see Choudhuri et al. 1993b), but for larger α (as in our solar case, Fig. 14) we find that the wake oscillates with a value somewhat, though not very, close to $\omega_{c_1} + \omega_{c_2}$. Presumably this frequency is due to coupling between different temperature layers.

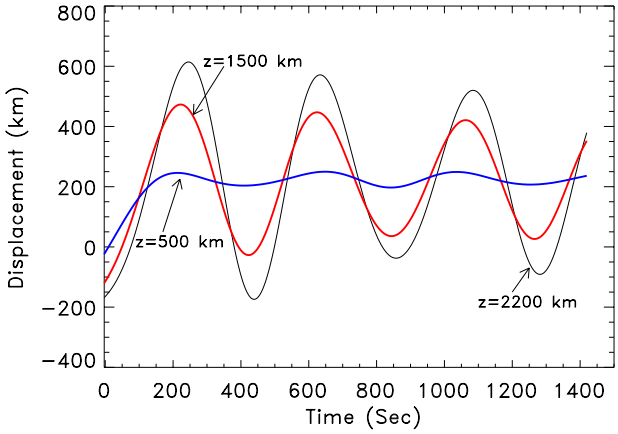

Fig. 14. Displacement of the flux tube as a function of time at various altitudes as indicated, with v_0, the maximum velocity of footpoint motion = 1.5 km s^{-1}, α, the measure of the thickness of the first layer = 3.34 and r, the measure of the temperature jump = 0.24

We have also studied the displacements of the flux tubes for a sharper temperature jump. These studies indicate that the amplitudes of the oscillations are then larger and grow faster and also last longer. A comparison of our numerical model with observations and their relevance will be discussed in the next section.

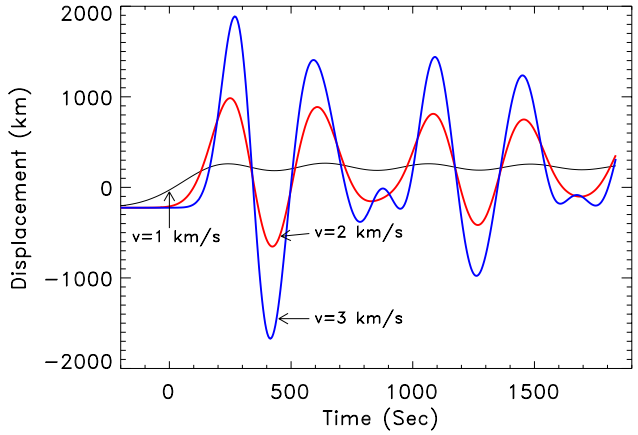

Fig. 15. Displacement of the flux tube as a function of time at a particular altitude ($h = 1800$ km), with different velocity of footpoint motions as indicated. Other parameters are the same as in Fig. 14

5. Discussion and conclusion

The salient feature of our observations is that we have detected intensity as well as velocity oscillations for very small regions of the network boundary, for a wide range of temperature lines starting from the low chromospheric, N I, to the transition region, O VI. Our results show that the variations are often intermittent, occurring only during part of the full time sequence. A power spectrum analysis picks out the periods that are present during the whole sequence and smear out periods that are present only during part of the sequence, whereas the method of wavelet analysis allowed us to study the duration as well as the periods of the oscillations. The significance test used here has enabled us to assign probability values to the detected frequencies/periods of oscillation, and thus has allowed us to judge which oscillations are or are not significant. We have shown that phase plots alone can be misleading at times especially for the detection of high frequency modes (as in the case of Mg X, Fig. 9). In a statistical sense, there are more velocity oscillations than intensity (as also reported by Hansteen et al. 2000). In general there are differences between network and internetwork behaviour. The internetwork behaviour re-confirms the recent findings by Wikstol et al. (2000), Hansteen et al. (2000), Cauzzi et al. (2000) and Judge et al. (2001), that the power extends upto 10 mHz (see Figs. 5 and 6). In this paper we have concentrated mainly on the network regions and find that there the power is concentrated around 3 mHz or lower. The wavelet spectra have revealed that these oscillations come in wave packets lasting for 10–20 mins. A similar sort of network behaviour is seen from the low chromospheric lines of e.g. N I up to the high transition region lines of e.g. O VI. For one particular case (see Figs. 12 and 13), where we found a confirmed influence of co-spatial magnetic field at the photospheric level we find similar velocity and intensity oscillations with strong power in the 2–2.5 mHz range for almost the entire observing period. These oscillations could be related to the impulsive motions at the photospheric level. The oscillations are considered to be due to waves, which are produced in short bursts with coherence time of about 10–20 min.

Earlier observers have interpreted the oscillations as being due to internal gravity waves (Damé et al. 1984; Lites 1984; Deubner & Fleck 1990; Kneer & von Uexküll 1993). Steffens et al. (1997) reported that the network oscillations are due to sausage modes compressing and heating network elements without vertical displacement. In a recent paper Kalkofen (1997) has interpreted the oscillations in the H and K lines of Ca II in network bright points as magneto-acoustic waves propagating upwards along thin flux tubes. Very recently Judge et al. (2001) have concluded that all the observed properties of the chromospheric dynamics points to the p-modes as the main driver of the dominant period. For the network regions Cauzzi et al. (2000) have reported a strong reduction of the amplitude of oscillations at the p-mode frequencies. Judge et al. (2001) have conjectured that some of the intermittency can be caused by the interaction of upward propagating waves with the magnetic field (which he describes as a magnetic shadow), which can also be responsible for the suppression of the intensity oscillations. Hansteen et al. (2000) have attributed some of the intermittency as being due to solar rotation and sit and stare effect. In general we also believe that the chromosphere and even the transition region oscillates primarily in response to forcing by p-modes. But it should be borne in mind also that they are often strongly influenced by the presence of the magnetic field at the boundaries of the network and also by the canopy field at chromospheric heights (important particularly for the internetwork regions). In the following paragraph we point out an alternative scenario which could be working for some network regions which have an underlying bright point at the photospheric level (detected as a network bright point, NBP, from the photospheric observations).

The numerical model presented here exhibits the qualitative nature of the oscillations. The theoretical frequency also indicates a strong coupling between the two idealized isothermal cavities, namely the chromospheric and coronal. The idealized model predicts a frequency for the flux tube oscillation at around 2.5 mHz, which falls within the observed range (see Figs. 12 and 13). Note that depending on the chosen value of β this can vary slightly. The scenario which we support here is that the jostling of the magnetic elements in the network boundary can excite oscillations in flux tubes, which can then in principle be an important mechanism for chromospheric and coronal heating. As kink waves excited at the photosphere travel upwards, their velocity amplitude increases (see Fig. 14). In chromospheric layers, the amplitude becomes comparable to the tube speed for kink waves, leading to an efficient coupling with sausage waves (Kalkofen 1997). Ziegler & Ulmschneider (1997) have studied the non-linear response to purely transverse foot-point shaking of a vertical magnetic flux tube. They have shown that the kink

waves of frequency ω_c can transfer energy to sausage type waves.Thus the signature of kink waves, their cut-off frequency, would be preserved in the transfer. These sausage waves may have been detected with the chromospheric and transition region lines (both in velocity and intensity signals) as reported here. The sausage waves can dissipate their energy by forming shocks (Zhugzhda et al. 1995), and thus can heat the upper layers of the solar atmosphere.

Finally we should remind the reader that we still do not have enough diagnostics to differentiate between wave modes. Complications arising as a result of the unknown topology of the magnetic field in the transition region would modify the interpretation of the data drastically. Thus we can only tentatively suggest that some of the network oscillations that we see in the 2–4 mHz range can be due to these magnetoacoustic waves. On a global scale the dominant dynamical effects in the chromospheric and transition region lines that we observe are most likely driven by the p-modes.

Acknowledgements. We would like to thank Bernhard Fleck for critical reading of the manuscript. Research at Armagh Observatory is grant-aided by the N. Ireland Dept. of Culture, Arts and Leisure, while partial support for software and hardware is provided by the STARLINK Project which is funded by the UK PPARC. This project was part funded by PPARC grant PPA/G/S/1999/00055. DB wishes to thank Drs. Arnab Rai Choudhuri and Mousumi Dikpati for using an earlier version of the numerical code for the modelling. DB is supported by ONDERZOEKSRAAD of K. U. Leuven (F/99/42). EOS is a member of the European Solar Magnetometry Network (`www.astro.su.se/dorch/esmn/`). CDS and SUMER are part of SOHO, the Solar and Heliospheric Observatory, which is a mission of international cooperation between ESA and NASA.

References

Berger, T. E., Schrijver, C. J., Shine, R. A., et al. 1995, ApJ, 454, 531
Berger, T. E., & Title, A. M. 1996, ApJ, 463, 49
Berger, T. E., Loefdahl, M. G., Richard S., & Title, A. M. 1998, ApJ, 495, 973
Cauzzi, G., Falchi, A., & Falciani, R. 2000, A&A, 357, 1093
Curdt, W., & Heinzel, P. 1998, ApJ, 503L, 95
Choudhuri, A. R., Auffret, H., & Priest, E. R. 1993a, Sol. Phys., 143, 49
Choudhuri, A. R., Dikpati, M., & Banerjee, D. 1993b, ApJ, 413, 811
Damé, L., Gouttebroze, P., & Malherbe, J. M. 1984, A&A, 130, 331
Deubner, F.-L., & Fleck, B. 1990, A&A, 228, 506
Dhillon, V. S., & Privett, G. J. 1997, Starlink User Note, 167.5
Doyle, J. G., O'Shea, E., van den Oord, G. H. J., & Banerjee, D. 1998, Sol. Phys., 181, 51
Doyle, J. G., van den Oord, G. H. J., O'Shea, E., & Banerjee, D. 1999, A&A, 347, 335
Fontela, J. M., Avrett, E. H., & Loeser, R. 1990, ApJ, 355, 700
Hansteen, V. H., Betta, R., & Carlsson, M. 2000, A&A, 360, 742
Hasan, S. S., & Kalkofen, W. 1999, ApJ, 519, 899
Harrison, R. Sawyer, E. C., Carter, M. K., et al. 1995, Sol. Phys., 162, 233
Judge, P., Carlsson, M., & Wilhelm, K. 1997, ApJL, 490, L195
Judge, P., Tarbell, T.D., & Wilhelm, K. 2001, ApJ, submitted
Kalkofen, W., Rossi, P., Bodo, G., & Massagali, S. 1994, A&A, 284, 976
Kalkofen, W. 1997, ApJ, 486, L145
Kneer, F., & von Uexküll , M. 1993, A&A, 274, 584
Lamb, H. 1932, in Hydrodynamics (Cambridge University Press, Cambridge)
Lites, B. W. 1984, ApJ, 277, 874
Lites, B. W., Rutten, R. J., & Kalkofen, W. 1993, ApJ, 414, 345
Muller, R., & Roudier, Th. 1992, Sol. Phys., 141, 27
Muller, R., Vigneau, J., Roudier, T., & Auffret, H. 1994, A&A, 283, 232
Nemec, A. F., & Nemec, J. M. 1985, AJ, 90, 2317
O'Shea, E. 1997, Ph.D. Thesis, Queens University of Belfast/Armagh Observatory
Pérez, E., 1999, Ph.D. Thesis, Queens University of Belfast/Armagh Observatory
Rae, I. C., & Roberts, B. 1982, ApJ, 256, 761
Roberts, B., & Ulmschneider, P. 1997, in Solar and Heliospheric Plasma Physics, ed. G. M. Simnett, C. E. Alissandrakis, & L. Vlahos, Lect. Notes Phys. 489 (Springer), 75
Spruit, H. C. 1981, A&A, 98, 155
Steffens, S., Deubner, F.-L., Fleck, B., et al. 1997, in 1st Advances in Solar Physics Euroconference, Advances in Physics of Sunspots, ed. B. Schmieder, J. C. del Toro Iniesta, & M. Vazquez, ASP Conf. Ser., 118, 284
Stenflo, J. O. 1994, in Solar Magnetic Fields (Dordrecht: Kluwer)
Torrence, C., & Compo, G. P. 1998, Bull. Amer. Meteor. Soc., 79, 61
Ulmschneider, P., Zähringer, K., & Musielak, Z. E. 1991, A&A, 241, 625
van Ballegooijen, A., Nisenson, P., Noyes, R. W., et al. 1998, ApJ, 509, 435
Wikstol, O., Hansteen, V. H., Carlsson, M., & Judge, P. G. 2000, ApJ, 531, 1150
Wilhelm, K., Curdt, W., Marsch, E., et al. 1995, Sol. Phys., 162, 189
Ziegler, U., & Ulmschneider, P. 1997, A&A, 324, 417
Zhugzhda, Y. D., Bromm, V., & Ulmschneider, P. 1995, A&A, 300, 302